Conjugated Zwitterionic Oligomers as Ligands on Perovskite Nanocrystals: Hybrid Structures with Tunable Interparticle Spacing

Christopher Cueto, Mingqiu Hu, Thomas P. Russell, and Todd Emrick*

Department of Polymer Science & Engineering, University of Massachusetts, Conte Center for Polymer Research. 120 Governors Dr, Amherst, MA 01003 (USA) E-mail: tsemrick@mail.pse.umass.edu

Perovskite, Nanoparticle, Conjugated Polymer, Zwitterion, Optoelectronic

ABSTRACT: Conventional ligands for $CsPbBr_3$ perovskite nanocrystals (NCs), composed of polar, coordinating head groups (*e.g.*, ammonium or zwitterionic) and aliphatic tails, are instrumental in stabilizing the NCs against sintering and aggregation. Nonetheless, the aliphatic (insulating) nature of these ligands represents drawbacks with respect to objectives in optoelectronics, and yet removing these ligands typically leads to loss of colloidal stability. In this paper, we describe the preparation of $CsPbBr_3$ NCs in the presence of discrete conjugated oligomers that were prepared by an iterative synthetic approach and capped at their chain-ends with sulfobetaine zwitterions for perovskite coordination. Notably, these zwitterionic oligofluorenes are compatible with the hot-injection and ligand exchange conditions used to prepare $CsPbBr_3$ NCs, yielding stable NC dispersions with high photoluminescence quantum yields (PLQY, >90%) and spectral features representative of both the perovskite core and conjugated ligand shell. Controlling the chain length of these capping ligands effectively regulated inter-NC spacing and packing geometry when cast into solid films, with evidence derived from both transmission electron microscopy (TEM) and grazing incidence x-ray scattering measurements.

INTRODUCTION

Lead halide perovskite nanocrystals (NCs) are an emerging class[1] of bright, narrow line-width nanoemitters that are especially unique for their soft, low energy ionic lattice,[2] and innate defect tolerance[3] that obviates the need for overcoating steps to achieve high photoluminescence quantum yields (PLQYs). Importantly, perovskite NC syntheses utilize abundant precursors (*e.g.* $PbBr_2$, CH_3NH_3Br, and Cs_2CO_3) that may be assembled *via* low-temperature ionic metathesis reactions[4,5] into a perovskite framework that— despite a proliferation of A-site (*e.g.* Cs^+) and X-site (*e.g.* Br^-) vacancies[6,7]—has exceptionally robust emission. As detailed by Protesescu, *et. al.*,[8] the emission wavelength of all-inorganic of $CsPbX_3$ NCs (where X = Cl, Br, I or combinations thereof) is tunable across the visible spectrum (ca. 400-700 nm) by changing the halide composition, with quantum size effects playing a lesser role for the most common NC morphologies (*i.e.* nanocubes with 10 nm edge lengths). Subsequently, $CsPbX_3$ NCs were found to participate in rapid anion (halide) exchange reactions[9,10] with their surroundings, enabled by their mobile, vacancy-laden halide sublattice,

thus opening routes to post-synthesis color tuning *via* simply mixing NCs with an external halide source (*e.g.* ammonium halides,[9-11] metal halide salts[9,10] or others[12,13]). This host of useful properties has driven studies of perovskite NCs in lasing,[14] detection and imaging,[15] photocatalysis,[16] quantum emitters[17] and LEDs,[18-20] where research continues at a rapid pace.

Semiconductor NCs as colloidal 'inks' are amenable to solution-casting, which is advantageous over high-temperature, vacuum deposition methods often needed for their bulk counterparts; however, a classic trade-off to their use in solid state devices is the presence of an insulating aliphatic ligand shell on their surface after synthesis. Ligands such as oleylamine and oleic acid are critical ingredients for NC synthesis —necessary to solubilize the Cs^+ and Pb^{2+} precursors and render the resulting $CsPbXr_3$ NCs colloidally stable—however they may create a dielectric barrier that impedes charge carrier mobility through NC films, especially when present in excess. Significant efforts[21-23] have been dedicated to refining the NC purification conditions to purge unbound ligand without compromising NC integrity. This is delicate

balance, as repetitive washing with polar solvents eventually removes the entire ligand shell (leading to sintering) and degrades the NC surface. The use of tight-binding ligands, such as *N,N*-dimethyl quaternary ammonium bromides[24] or zwitterions,[25] has helped to address these NC stability issues, permitting precipitation steps to reduce ligand concentrations down to an approximately single-layer thick coating. Going further, several groups reported strategies to eliminate all long-chain aliphatic ligands, including: *a)* resurfacing the NCs with an inorganic salt shell solely comprised of Na^{+} and Br^{-} ions, which dramatically enhanced charge carrier mobility in NC-based LEDs,[20] and *b)* using aromatic ligands such as anilinium,[18] benzyl and phenalkylammonium,[26,27] and cinnamyl ammonium,[28] much in the same way that π-conjugated ligands were previously combined with metal chalcogenide QDs.[29-31] This latter approach has shown promise in devices, in terms of lower turn-on voltages and improved efficiencies. However, the cited examples have a limited extent of π-conjugation and rely on weak binding ammonium and anilinium cations to bring the aromatic ligands into close association with the perovskite surface. Other examples include our own group's work on benzyl ammonium-containing conjugated polymers used to grow CsPbBr$_3$ NCs,[32] as well as a study by Liang, *et. al.* wherein CsPbBr$_3$ NCs were grown in a nanoreactor comprised of poly(3-hexylthiophene) tethered to the chain-ends of a polyacrylic acid star polymer.[33] While there are obvious motivations for merging the excellent optoelectronic properties of lead halide perovskites and π-conjugated polymers and oligomers, at present there is a limited understanding of the interface between these material classes, which in turn is due to the limited synthetic tools available to access them.

Zwitterions exhibit exceptionally tight coordination to lead halide perovskite surfaces—a feature attributed to simultaneous binding (*i.e.* chelation) of the zwitterion cation and anion head groups to adjacent pairs of A- and X-site vacancies.[25] By comparison, more conventional ligands such as primary ammonium halide salts exist in a state of dynamic exchange with CsPbBr$_3$ surfaces and can easily desorb following multiple NC precipitations into polar solvent.[34] Conjugated polymer zwitterions (CPZs) are therefore a natural pairing with perovskite NCs, conferring strong stability and anchoring the conjugated backbone in close proximity with the perovskite surface. The CPZs previously reported by our group[35-38] and others[39,40] contain multiple zwitterions along the polymer chain, and as such they dissolve as aqueous solutions or in polar organic solvents. This solubility is favorable for high fidelity interlayers of organic photovoltaic (OPV) devices[41] but problematic for perovskite NCs which require low polarity solvents such as hexanes or toluene. Relocating the zwitterions to the polymer chain-end will produce structures that combine the ligand coordination of zwitterions with apolar solvent compatibility. Along these lines, we report the first examples of conjugated oligomers/polymers (based on oligofluorene chains) with ω-chain-end sulfobetaine groups positioned in close proximity to the conjugated backbone. This new class of CPZs is readily integrated into existing procedures for CsPbBr$_3$ NC synthesis and ligand exchange, delivering perovskite NCs with an intimately attached, single-layer of wide band gap semiconductor ligands.

RESULTS & DISCSUSSION

Sulfobetaine (SB)-terminated oligofluorene ligands (*n* = 1-4) were prepared in two stages: 1) a series of iterative Suzuki couplings (**Scheme 1a**) to generate the oligofluorene chain and 2) reductive amination and ring-opening at the chain-end to furnish the SB zwitterion (**Scheme 1b**). Key to this strategy was the use of *N*-methylimidodiacetic acid (MIDA) as the boronic acid protecting group in Suzuki-Miyaura (SM) cross coupling. Under anhydrous SM conditions, free boronic acids reacted selectively in the presence of their MIDA-complexed counterparts,
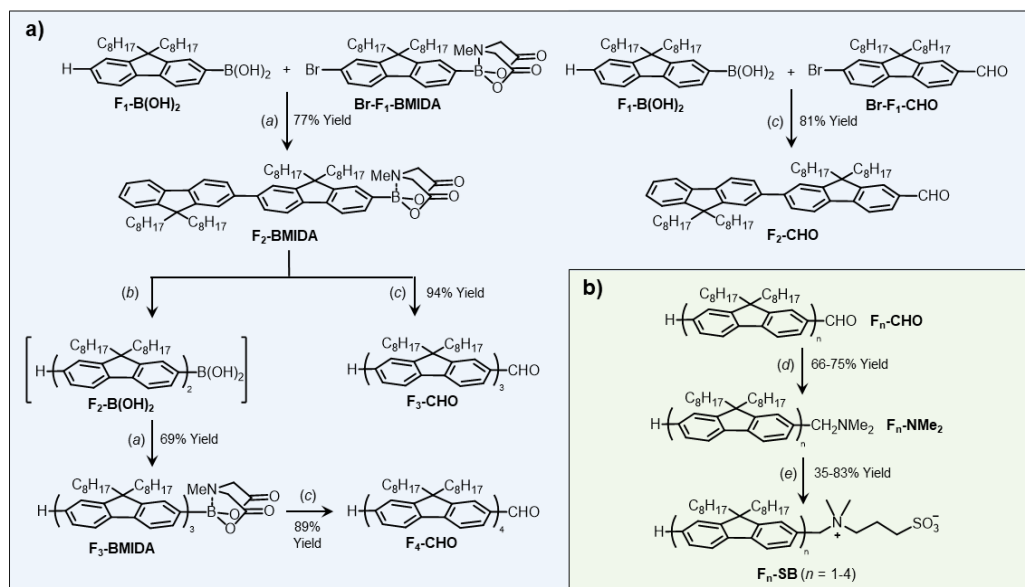
with the MIDA group removed later by stirring in aqueous base. Using MIDA-protected *halo*boronic acids (*e.g.* **Br-F₁-BMIDA**, **Scheme 1a**), repeated coupling and deprotection results in step-by-step growth of complex polyaromatic scaffolds,[42–44] an example being the sequence-defined, regiospecific π-conjugated polymers recently reported by Xu, *et. al.*[45] The MIDA-protection strategy was selected for this work owing to its relatively high throughput and ease of purification,[46] good control over chain length and an ability to differentiate the chemistry of the α and [...]

coupling of 9,9'-dioctylfluorene-2-boronic acid (**F₁-B(OH)₂**) with the MIDA-protected 2-bromo-9,9'-dioctylfluorene-7-boronic acid (**Br-F₁-BMIDA**). The latter was synthesized in two steps from 2,7-dibromo-9,9'-dioctylfluorene *via* borylation and MIDA-protection, giving monomer **Br-F₁-BMIDA** in good yield (71%) on a multigram scale. The **F₁-B(OH)₂** + **Br-F₁-BMIDA** SM cross-coupling gave the dimer **F₂-BMIDA** in good yield (77%), which was either chain-capped with 2-bromo-9,9'-di-*n*-octylfluorene-7-carboxaldehyde (**Br-F₁-CHO**) to produce a trimer with chain-end aldehyde (**F₃-CHO**) or advanced into further iterations of chain growth. Using fluorene-based chain-capping reagents **F₁-B(OH)₂** and **Br-F₁-CHO** (as opposed to simpler boronic acids such as *p*-tolylboronic acid[45]) reduced (by 2x) the number deprotection and coupling iterations needed to reach the target oligomer, thus simplifying the process. Chain elongation of **F₂-BMIDA** proceeded by stirring the dimer as a solution in degassed THF with NaOH(aq), converting the MIDA group to the free boronic acid **F₂-B(OH)₂**, which was then coupled with **Br-F₁-BMIDA** to afford **F₃-BMIDA** (69% yield). Both **F₂-BMIDA** and **F₃-BMIDA** were capped with **Br-F₁-CHO** by reacting the MIDA-protected oligomers under *aqueous* SM coupling conditions, using K₂CO₃(aq) to both remove the MIDA protecting groups *in situ*[48,49] and activate the resulting boronic acid. Chain-capping in this manner afforded the tri- (**F₃-CHO**, 94% yield) and tetrameric (**F₄-CHO**, 89% yield) aldehydes, respectively; similar chemistry whereby the **F₁-B(OH)₂** and **Br-F₁-CHO** chain cappers were coupled directly furnished the dimer aldehyde (**F₂-CHO**, 81% yield). The unimer, 9,9'-dioctylfluorene-2-carboxaldehyde (**F₁-CHO**), was synthesized *via* formylation of 9,9'-dioctyl 9,9'-dioctyl-2-bromofluorene based on previously reported methods.[50] While the tetramer was the longest ligand we prepared, in principle this iterative strategy may be repeated to reach longer chain lengths, noting that oligofluorenes reach full conjugation length at DP ~6.[51]

Conversion of the chain-end aldehydes of the **F₁-CHO** through **F₄-CHO** series to SB groups was
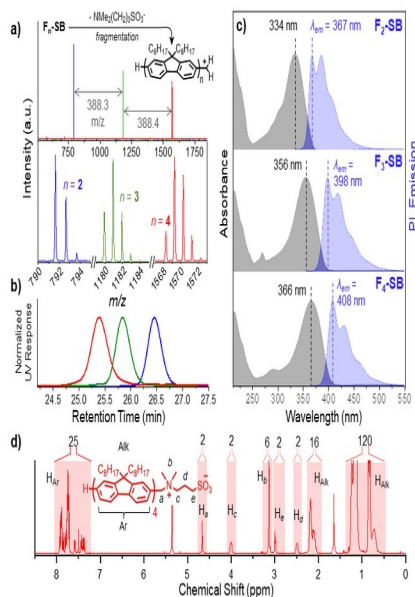
accomplished in two steps: 1) reductive amination with HNMe₂/Ti(O*i*Pr)₄ followed by addition of NaBH₄,[52] effecting aldehyde to *N*,N-dimethylamine conversion (**Fₙ-NMe₂**) and 2) ring-opening of 1,3-propanesultone with the **Fₙ-NMe₂** oligomers. This yielded the corresponding **Fₙ-SB** zwitterions as solid powders that dissolved easily in toluene or CHCl₃—useful solvents for performing experiments with perovskite NCs. MALDI-TOF and GPC confirmed the discrete chain lengths of these zwitterionic oligofluorenes; in MALDI-TOF, an [M – (CH₃)₂N(CH₂)₃SO₃]⁺ mass

Figure 1 Characterization of zwitterionic oligofluorene ligands. a) MALDI-TOF mass data show single peaks corresponding to a mass fragment originating from loss of NMe₂(CH₂)₃SO₃⁻. b) narrow elution profiles observed by gel permeation chromatography (GPC) in THF confirm the uniform and increasing chain length for each oligomer (F₂ → F₄). c) overlayed UV-vis and PL spectra. PL spectra were recorded with excitation wavelengths set to the labeled absorption maximum of each oligomer. d) ¹H NMR (500 MHz, CD₂Cl₂) of the F₄-SB ligand fragment (corresponding to a benzylic cation generated by loss of *N*,N-dimethylaminopropyl sulfonate) was observed for all **Fₙ-SB**. The SB resonances were visible by ¹H NMR spectroscopy in CD₂Cl₂ (4.67, 4.00, 3.00, 3.14 and 2.49 ppm), with integration against the aromatic protons (7.3-8.0 ppm) consistent with the expected chain length. UV-vis and PL spectra of solutions of **F₂-SB** through **F₄-SB** in THF showed a shift in absorption (334-381 nm) and PL emission maxima (367-408 nm) to longer wavelengths with increasing *n*, resembling the known optical properties of non-functionalized oligofluorenes.[51]

The **Fₙ-SB** oligomers with their zwitterion 'head' and conjugated 'tail'—flanked by pairs of *n*-octyl chains on each repeat unit—resemble conventional zwitterionic surfactants,[25,53,54] and we found them useful in both the NC synthesis
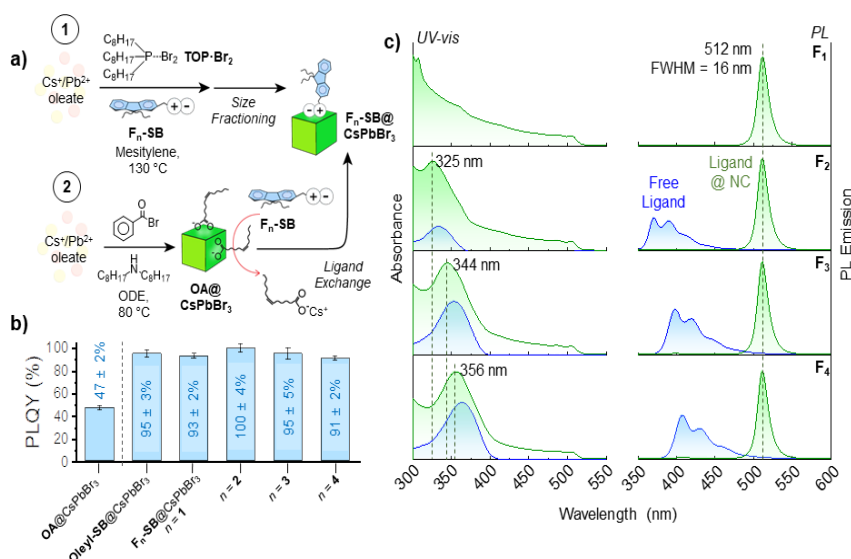
and ligand exchange. Adding F_n-SB directly to the CsPbBr$_3$ NC growth procedure was enabled by the excellent solubility of the F_n-SB oligomers in high boiling solvents, such as mesitylene, used in the colloidal hot-injection. In a typical procedure, the F_n-SB ligand was dissolved in a mesitylene solution of cesium and lead oleate salts and heated to 130 °C, followed by injection of a tri-*n*-octylphosphine·Br$_2$ complex (TOP·Br$_2$) to form CsPbBr$_3$. The resulting F_n-SB@CsPbBr$_3$ NCs tend to have a wide range of initial shapes and sizes, typical of these zwitterion-based methods.[54] Size-selective precipitation was performed by washing the F_n-SB@CsPbBr$_3$ solution with acetone in small increments; for F_1-SB@CsPbBr$_3$ NCs, this resulted in multiple size fractions with edge lengths in the range of 6-8 nm, PL emission centered between 495-507 nm (FWHM = 20-21 nm), and a total combined CsPbBr$_3$ yield of 75%. Similar results were obtained using the F_2-SB through F_4-SB ligands, though longer ligands tended to produce smaller NCs that deviated from a cuboidal morphology, and accurate determination of PLQY was challenging in some cases. Overall, this method still produced high-quality, brightly fluorescent CsPbBr$_3$ NCs surface-functionalized with F_n-SB oligomers.

We also studied ligand exchange, using F_n-SB ligands and CsPbBr$_3$ NCs. The NCs used in these experiments were prepared using the secondary amine method of Imran,[55] which gives an oleate-rich ligand. Replacing primary amines (*e.g.*, oleylamine) in typical CsPbX$_3$ syntheses[8,12]— where their reversible surface binding as protonated ammonium salts is thought to promote anisotropic growth[55,56] and give mixtures of nanocubes and platelets—with secondary amines (*e.g.* dioctylamine, DOAm), which bind CsPbX$_3$ less effectively, improves NC shape and size homogeneity.[55] In addition, the oleate coating on these NCs is readily displaced by other ligands, for example quaternary ammonium halides,[57] resulting in efficient exchange. In our hands, the synthesis of oleate-capped CsPbBr$_3$ NCs gave size uniform nanocubes (8.4 ± 0.5 nm) with narrow PL emission (FWHM = 17 nm) centered at 511 nm, and moderate PLQY (47 ± 2%). Remarkably, adding small amounts of the F_n-SB zwitterions (0.2-0.6 mg F_n-SB/mg CsPbBr$_3$, corresponding to ~1.3 ligands·nm^{-2}) to these oleate-capped NCs, followed by stirring and precipitation into acetone, resulted in a dramatic PLQY boost (91-99%). A similar surface passivation and PL brightening was observed when adding oleyl sulfobetaine (oleyl-SB), demonstrating the impact of zwitterion head group in perovskite surface stabilization. Control experiments, performed by omitting the zwitterion and precipitating the oleate-capped NCs directly into acetone, yielded a yellow, non-luminescent precipitate that failed to redisperse in toluene. After two ligand exchange steps, it is possible to reduce the residual oleic acid/oleate concentration to 0.1 mM, comprising ≤ 10% of the resulting ligand shell; notably, despite the different sizes of F_1-SB through F_4-SB, their grafting density on the CsPbBr$_3$ surface is approximately the same (ρ = 1.0 – 1.3 ligands·nm^{-2}, determined by quantitative NMR spectroscopy performed on digested NC samples using 1,2,4,5-tetrachloro-3-nitrobenzene as internal standard). Compared to F_n-SB@CsPbBr$_3$ NCs prepared by direct synthesis, the NCs produced by ligand exchange have a more consistent morphology and were easier to isolate and characterize, and all of the following examples of F_n-SB@CsPbBr$_3$ NCs in the text were prepared *via* this method.

Inspection of the UV-vis absorbance spectra in the F_n-SB@CsPbBr$_3$ NC series shows composite features of both the oligofluorene shell and the underlying CsPbBr$_3$ core (**Figure 2**). However, excitation of these F_n-SB@CsPbBr$_3$ NCs at the absorption maximum of the conjugated ligand (307-366 nm) produced PL spectra dominated by CsPbBr$_3$ emission, with only trace detectable oligofluorene PL. PL spectra of F_2-SB (free ligand) and F_2-SB@CsPbBr$_3$ (NC-bound ligand) solutions (prepared at the same mg/mL ligand concentration, **Figure 2**) illustrate the order-of-magnitude extent of ligand PL suppression in the

Examining the F_n-SB@CsPbBr$_3$ NCs by transmission electron microscopy (TEM) revealed preservation of the cuboidal morphology after ligand exchange, although in the case of F_4-SB@CsPbBr$_3$ the edges of the cubes are less well-defined. Image analysis of F_1-SB@CsPbBr$_3$ through F_4-SB@CsPbBr$_3$ showed similar size (edge length) of individual NCs across the entire series (d$_{NC}$ = ca. 9 nm), consistent with the similar PL emission wavelength (512 nm) associated with the perovskite core for all F_n-SB@CsPbBr$_3$ samples. Closer inspection of the TEM images in **Figure 3** shows that longer ligands produce
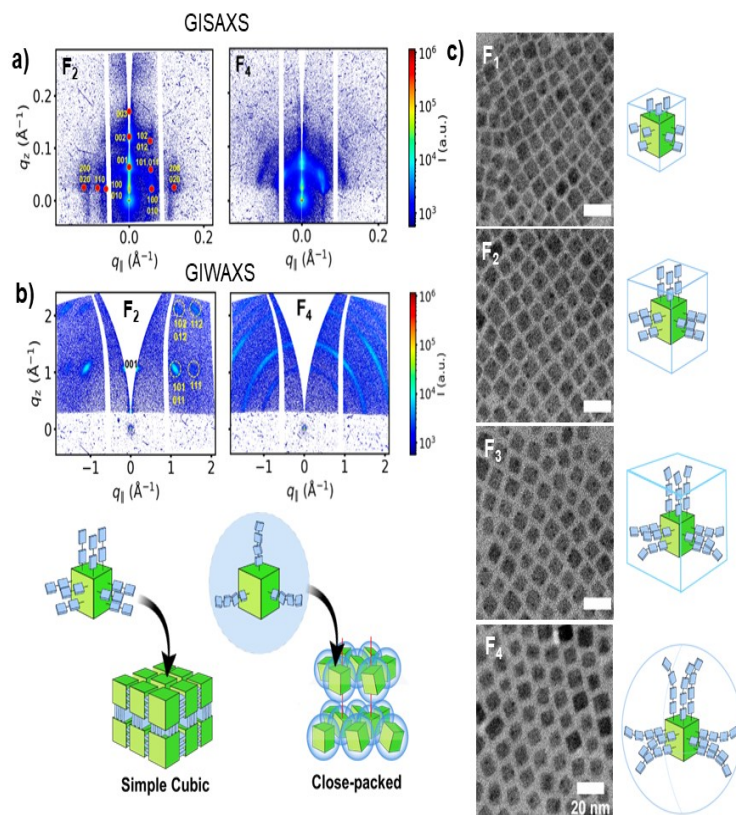

Figure 3 a) GISAXS measurements F_n-SB@CsPbBr$_3$ NCs n = 1-4 prepared via ligand exchange on OA@CsPbBr$_3$ NCs, cast as a film on silicon substrate, which show a gradual shift in the distance between packing planes in the in-plane scattering direction as well as a transition from simple cubic to close-packed arrangement of the NCs in the film. b) azimuthal broadening for the F_4-SB@CsPbBr$_3$ NC film suggests that the longer ligand disrupts any orientational preference of the NC with respect to the underlying substrate. c) TEM of these same NCs showing increasing inter-NC distances as a result of increasing conjugation length of ligand

systematically larger inter-NC spacing, as well as different NC arrangements (cubic with shorter ligands *vs*. hexagonal with longer ligands) as they array in a single layer on the TEM grid. These observations suggest that longer ligands disrupt the alignment between adjacent NC facets and override the innate packing tendency of hard

Figure 4 a) Confocal fluorescence microscope images of superstructures formed from F_2-SB@CsPbBr$_3$ NCs. Polarized optical light microscope image (b) of one of these isolated super-structures on Si wafer. AFM phase (c) and height retrace (d) giving approximate dimensions of 16x19x0.5 μm for the assembled structure.

nanocubes. Further insights were gained from

grazing incidence small angle x-ray scattering (GISAXS) of concentrated F_n-SB@CsPbBr$_3$ NC solutions drop-cast onto polished Si (**Figure 3**). Both **F_1-SB@CsPbBr$_3$** and **F_2-SB@CsPbBr$_3$** formed films with simple cubic packing, with the latter exhibiting the most regular cubic structure. Indexing of the GISAXS for **F_2-SB@CsPbBr$_3$** NCs using a primitive cubic lattice is shown in **Figure 3**. A gradual transition in the packing geometry was observed for films of **F_3-SB@CsPbBr$_3$**, where the scattering pattern reflects the presence of mixed domains with cubic and close-packed (*i.e.* face-centered cubic or hexagonal close packed) geometry. For NCs capped with **F_4-SB@CsPbBr$_3$**, the film exclusively shows a close-packed hexagonal structure, potentially due to the longer ligands projecting from the NC surface that make it present as a soft or 'fuzzy' sphere instead of a hard cube. It is also possible that the loss of nanocube edge definition (as noted above for **F_4-SB@CsPbBr$_3$**) contributes to changes in packing geometry. In-plane scattering was used to estimate the nearest neighbor distances for these samples, taking into account the differences in film morphology. For **F_1-SB@CsPbBr$_3$** through **F_3-SB@CsPbBr$_3$**, a simple cubic packing was assumed and the nearest neighbor distance was estimated simply as $\delta = a_{sc} - d_{NC}$, whereas for **F_4-SB@CsPbBr$_3$** hexagonal packing was assumed with a nearest neighbor distance of $\delta = ((3)^{1/2}/2)a_{hp} - d_{NC}$ (where a_{sc} and a_{hp} are the average distances between packing planes for cubic and hexagonal-packed structures—calculated as $2\pi/q^*$, with q^* being the primary scattering vector—and d_{NC} is the cube edge length estimated by TEM). We find that the values of δ trend from 1.0, 1.6, 3.3 and 4.1 nm for **F_1-SB@CsPbBr$_3$** through **F_4-SB@CsPbBr$_3$**, consistent with the spacings observed by TEM. Given that the monomer length of a single fluorene repeat unit is estimated[59] to be 7.5 Å (and assuming the ligands exist on the NC surface as fully extended rigid rods), the inter-NC spacings derived from TEM and x-ray scattering imply interdigitation of the conjugated ligands between adjacent NCs, or that the chain axis of the oligofluorene backbone does not extend normal to the NC surface. Grazing incidence wide-angle x-ray diffraction (GIWAXD) measurements on this same series of samples shows no azimuthal broadening of the diffractions for **F_n-SB@CsPbBr$_3$** NC films when n = 1 or 2, suggesting the (001) plane of the cubic CsPbBr$_3$ crystal lattice aligns parallel with the Si substrate (*i.e.* the cubic NCs align face on with the substrate). The indexing of diffractions reflections using primitive cubic lattice is marked in Figure 3 (b). The ratio between the scattering vector of those diffractions turns out to be 1:√2:√3:2: √5: √6, arising from crystal planes (001), (101) or (011), (111), (012) or (102), and (112), accordingly, confirming the face-on orientation of the NC on the substrate. The face-on orientation

of NCs on the substrate allowed the third index, l of (hkl), to be identified unambiguously. The first two indices, h and k, are not distinguishable due to NC freely rotating along the normal direction of the substrate. On the contrary, for **F_n-SB@CsPbBr$_3$** NC films, where n = 3 or 4, there is significant azimuthal broadening, as longer ligands disrupt any orientational preference of the NCs with respect to the underlying substrate. While the results for **F_1-SB** and **F_2-SB@CsPbBr$_3$** NCs were consistent with previous studies showing packing of aliphatic ligand-capped perovskite nanocubes into well-ordered cubic superlattices,[60,61] clearly the longer ligands disrupt face-on inter-NC and NC-substrate alignment.

Notably, casting **F_2-SB@CsPbBr$_3$** NC films under slightly different conditions (higher dilution on silylated glass) produced brightly fluorescent, micron-sized rectangles that were observable by confocal microscopy (**Figure 4**). These resemble the types of structures previously reported for perovskite NC superlattices, which have drawn interest due to their properties of collective emission (*i.e.* coherent coupling between quantum emitters in a long range-ordered, closely packed lattice that causes them to collectively behave as a large, single emitting dipole that releases a burst of superfluorescent radiation).[61,62] Similar observations were made for NCs with **F_3-SB** and **F_4-SB** ligands (**Figures S18 and S19**), with superlattice formation enriched at
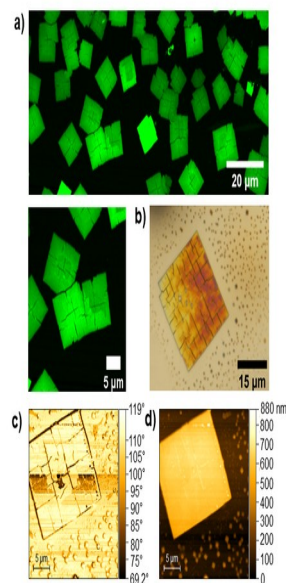
the edge of the drying droplet (unlike the samples in **Figure 3**, which deposited as a uniform film on Si wafer). No such superstructures formed with **F_1-SB** or **oleyl-SB**, and it is possible that the extended conjugated backbone in longer ligands in some way directs NC assembly (*e.g.* π-π stacking interactions). AFM imaging of an isolated

F₂-SB@CsPbBr₃ superstructure in **Figure 4** shows that the lateral dimensions (16 x 19 μm) are significantly larger than its height (0.5 μm, *c.a.* 47 layers of **F₂-SB@CsPbBr₃** NCs based on the in-plane *d* spacing, 10.6 nm, determined from GISAXS above).

CONCLUSIONS

A new series of π-conjugated ligands were prepared in good yields *via* an iterative synthesis strategy, giving precise, zwitterion-capped, oligomeric structures that proved compatible with existing methods for perovskite NC hot-injection and ligand exchange. Compared with prior reports of conjugated polymer/oligomer zwitterions, repositioning the zwitterion to the chain-end renders these structures soluble in the solution media needed to grow and handle $CsPbBr_3$ NCs (*i.e.* non-polar hydrocarbons). Assuming chelation of the zwitterion chain-end with perovskite surface, the placement of zwitterion positions the π-conjugated ligand backbone in close proximity to the NC, promoting electronic communication between the two. The deep suppression of ligand PL in the presence of NC may be indicative of such communication, and the range of oligofluorene chain lengths surveyed here are short of the full conjugation length, resulting in a range of ligand band energies for pairing with the perovskite core. The variable chain lengths also leverage control over the inter-NC spacing and packing geometry when cast into thin films, in some cases forming micron-sized structures reminiscent of perovskite NC superlattices reported elsewhere in the literature. While oligofluorene backbones were used here due to their characteristically wide bandgaps and low-lying HOMO levels (making them suitable for funneling injected charge carriers into the $CsPbBr_3$ core for light-emission), the synthesis methods described in this paper are adaptable to other types of polyaromatic chains. We envision this as a general strategy for merging perovskite and organic semiconductors into hybrid structures with tunable electronic properties based on ligand chemistry (*i.e.* monomer choice, chain length) that can be tailored to suit their target applications, such as light-emission, light-harvesting or photocatalysis.

ASSOCIATED CONTENT

Details of all ligand, nanocrystal syntheses, ligand exchange procedures, and substrate/sample preparation for characterization are given in the supporting information. This material is available free of charge via the Internet at http://pubs.acs.org.

AUTHOR INFORMATION

Corresponding Author

* email: tsemick@mail.pse.umass.edu

REFERENCES

(1) Dey, A.; Ye, J.; De, A.; Debroye, E.; Ha, S. K.; Bladt, E.; Kshirsagar, A. S.; Wang, Z.; Yin, J.; Wang, Y.; Quan, L. N.; Yan, F.; Gao, M.; Li, X.; Shamsi, J.; Debnath, T.; Cao, M.; Scheel, M. A.; Kumar, S.; Steele, J. A.; Gerhard, M.; Chouhan, L.; Xu, K.; Wu, X.; Li, Y.; Zhang, Y.; Dutta, A.; Han, C.; Vincon, I.; Rogach, A. L.; Nag, A.; Samanta, A.; Korgel, B. A.; Shih, C.-J.; Gamelin, D. R.; Son, D. H.; Zeng, H.; Zhong, H.; Sun, H.; Demir, H. V.; Scheblykin, I. G.; Mora-Seró, I.; Stolarczyk, J. K.; Zhang, J. Z.; Feldmann, J.; Hofkens, J.; Luther, J. M.; Pérez-Prieto, J.; Li, L.; Manna, L.; Bodnarchuk, M. I.; Kovalenko, M. V.; Roeffaers, M. B. J.; Pradhan, N.; Mohammed, O. F.; Bakr, O. M.; Yang, P.; Müller-Buschbaum, P.; Kamat, P. V.; Bao, Q.; Zhang, Q.; Krahne, R.; Galian, R. E.; Stranks, S. D.; Bals, S.; Biju, V.; Tisdale, W. A.; Yan, Y.; Hoye, R. L. Z.; Polavarapu, L. State of the Art and Prospects for Halide Perovskite Nanocrystals. *ACS Nano* **2021**, *15* (7), 10775–10981. https://doi.org/10.1021/acsnano.0c08903.

(2) Glasser, L. Lattice Energies of Crystals with Multiple Ions: A Generalized Kapustinskii Equation. *Inorg. Chem.* **1995**, *34* (20), 4935–4936. https://doi.org/10.1021/ic00124a003.

(3) Kang, J.; Wang, L.-W. High Defect Tolerance in Lead Halide Perovskite CsPbBr3. *J. Phys. Chem. Lett.* **2017**, *8* (2), 489–493. https://doi.org/10.1021/acs.jpclett.6b02800.

(4) Zhang, F.; Zhong, H.; Chen, C.; Wu, X.; Hu, X.; Huang, H.; Han, J.; Zou, B.; Dong, Y. Brightly Luminescent and Color-Tunable Colloidal CH3NH3PbX3 (X = Br, I, Cl) Quantum Dots: Potential Alternatives for Display Technology. *ACS Nano* **2015**, *9* (4), 4533–4542. https://doi.org/10.1021/acsnano.5b01154.

(5) Li, X.; Wu, Y.; Zhang, S.; Cai, B.; Gu, Y.; Song, J.; Zeng, H. CsPbX3 Quantum Dots for Lighting and Displays: Room-Temperature Synthesis, Photoluminescence Superiorities, Underlying Origins and White Light-Emitting Diodes. *Advanced Functional Materials* **2016**, *26* (15), 2435–2445. https://doi.org/10.1002/adfm.201600109.

(6) Walsh, A.; Scanlon, D. O.; Chen, S.; Gong, X. G.; Wei, S.-H. Self-Regulation Mechanism for Charged Point Defects in Hybrid Halide Perovskites. *Angewandte Chemie International Edition* **2015**, *54* (6), 1791–1794. https://doi.org/10.1002/anie.201409740.

(7) Kovalenko, M. V.; Protesescu, L.; Bodnarchuk, M. I. Properties and Potential Optoelectronic Applications of Lead Halide Perovskite Nanocrystals. *Science* **2017**, *358* (6364), 745–750. https://doi.org/10.1126/science.aam7093.

(8) Protesescu, L.; Yakunin, S.; Bodnarchuk, M. I.; Krieg, F.; Caputo, R.; Hendon, C. H.; Yang, R. X.; Walsh, A.; Kovalenko, M. V. Nanocrystals of Cesium Lead Halide

Perovskites (CsPbX3, X = Cl, Br, and I): Novel Optoelectronic Materials Showing Bright Emission with Wide Color Gamut. *Nano Lett.* **2015**, *15* (6), 3692–3696. https://doi.org/10.1021/nl5048779.

(9) Nedelcu, G.; Protesescu, L.; Yakunin, S.; Bodnarchuk, M. I.; Grotevent, M. J.; Kovalenko, M. V. Fast Anion-Exchange in Highly Luminescent Nanocrystals of Cesium Lead Halide Perovskites (CsPbX3, X = Cl, Br, I). *Nano Lett.* **2015**, *15* (8), 5635–5640. https://doi.org/10.1021/acs.nanolett.5b02404.

(10) Akkerman, Q. A.; D'Innocenzo, V.; Accornero, S.; Scarpellini, A.; Petrozza, A.; Prato, M.; Manna, L. Tuning the Optical Properties of Cesium Lead Halide Perovskite Nanocrystals by Anion Exchange Reactions. *J. Am. Chem. Soc.* **2015**, *137* (32), 10276–10281. https://doi.org/10.1021/jacs.5b05602.

(11) Cueto, C.; Hu, W.; Ribbe, A.; Bolduc, K.; Emrick, T. Polystyrene-Based Macromolecular Ammonium Halides for Tuning Color and Exchange Kinetics of Perovskite Nanocrystals. *Angewandte Chemie International Edition* **2022**, *61* (37), e202207126. https://doi.org/10.1002/anie.202207126.

(12) Imran, M.; Caligiuri, V.; Wang, M.; Goldoni, L.; Prato, M.; Krahne, R.; De Trizio, L.; Manna, L. Benzoyl Halides as Alternative Precursors for the Colloidal Synthesis of Lead-Based Halide Perovskite Nanocrystals. *J. Am. Chem. Soc.* **2018**, *140* (7), 2656–2664. https://doi.org/10.1021/jacs.7b13477.

(13) Creutz, S. E.; Crites, E. N.; De Siena, M. C.; Gamelin, D. R. Anion Exchange in Cesium Lead Halide Perovskite Nanocrystals and Thin Films Using Trimethylsilyl Halide Reagents. *Chem. Mater.* **2018**, *30* (15), 4887–4891. https://doi.org/10.1021/acs.chemmater.8b02100.

(14) Zhu, H.; Fu, Y.; Meng, F.; Wu, X.; Gong, Z.; Ding, Q.; Gustafsson, M. V.; Trinh, M. T.; Jin, S.; Zhu, X.-Y. Lead Halide Perovskite Nanowire Lasers with Low Lasing Thresholds and High Quality Factors. *Nature Mater* **2015**, *14* (6), 636–642. https://doi.org/10.1038/nmat4271.

(15) Wei, H.; Fang, Y.; Mulligan, P.; Chuirazzi, W.; Fang, H.-H.; Wang, C.; Ecker, B. R.; Gao, Y.; Loi, M. A.; Cao, L.; Huang, J. Sensitive X-Ray Detectors Made of Methylammonium Lead Tribromide Perovskite Single Crystals. *Nature Photon* **2016**, *10* (5), 333–339. https://doi.org/10.1038/nphoton.2016.41.

(16) Huynh, K. A.; Nguyen, D. L. T.; Nguyen, V.-H.; Vo, D.-V. N.; Trinh, Q. T.; Nguyen, T. P.; Kim, S. Y.; Le, Q. V. Halide Perovskite Photocatalysis: Progress and Perspectives. *Journal of Chemical Technology & Biotechnology* **2020**, *95* (10), 2579–2596. https://doi.org/10.1002/jctb.6342.

(17) Utzat, H.; Sun, W.; Kaplan, A. E. K.; Krieg, F.; Ginterseder, M.; Spokoyny, B.; Klein, N. D.; Shulenberger, K. E.; Perkinson, C. F.; Kovalenko, M. V.; Bawendi, M. G. Coherent Single-Photon Emission from Colloidal Lead Halide Perovskite Quantum Dots. *Science* **2019**, *363* (6431), 1068–1072. https://doi.org/10.1126/science.aau7392.

(18) Chiba, T.; Hayashi, Y.; Ebe, H.; Hoshi, K.; Sato, J.; Sato, S.; Pu, Y.-J.; Ohisa, S.; Kido, J. Anion-Exchange Red Perovskite Quantum Dots with Ammonium Iodine Salts for Highly Efficient Light-Emitting Devices. *Nature Photon* **2018**, *12* (11), 681–687. https://doi.org/10.1038/s41566-018-0260-y.

(19) Chen, H.; Fan, L.; Zhang, R.; Bao, C.; Zhao, H.; Xiang, W.; Liu, W.; Niu, G.; Guo, R.; Zhang, L.; Wang, L. High-Efficiency Formamidinium Lead Bromide Perovskite Nanocrystal-Based Light-Emitting Diodes Fabricated via a Surface Defect Self-Passivation

Strategy. *Advanced Optical Materials* **2020**, *8* (6), 1901390. https://doi.org/10.1002/adom.201901390.

(20) Dong, Y.; Wang, Y.-K.; Yuan, F.; Johnston, A.; Liu, Y.; Ma, D.; Choi, M.-J.; Chen, B.; Chekini, M.; Baek, S.-W.; Sagar, L. K.; Fan, J.; Hou, Y.; Wu, M.; Lee, S.; Sun, B.; Hoogland, S.; Quintero-Bermudez, R.; Ebe, H.; Todorovic, P.; Dinic, F.; Li, P.; Kung, H. T.; Saidaminov, M. I.; Kumacheva, E.; Spiecker, E.; Liao, L.-S.; Voznyy, O.; Lu, Z.-H.; Sargent, E. H. Bipolar-Shell Resurfacing for Blue LEDs Based on Strongly Confined Perovskite Quantum Dots. *Nat. Nanotechnol.* **2020**, *15* (8), 668–674. https://doi.org/10.1038/s41565-020-0714-5.

(21) Li, J.; Xu, L.; Wang, T.; Song, J.; Chen, J.; Xue, J.; Dong, Y.; Cai, B.; Shan, Q.; Han, B.; Zeng, H. 50-Fold EQE Improvement up to 6.27% of Solution-Processed All-Inorganic Perovskite CsPbBr3 QLEDs via Surface Ligand Density Control. *Advanced Materials* **2017**, *29* (5), 1603885. https://doi.org/10.1002/adma.201603885.

(22) Chiba, T.; Hoshi, K.; Pu, Y.-J.; Takeda, Y.; Hayashi, Y.; Ohisa, S.; Kawata, S.; Kido, J. High-Efficiency Perovskite Quantum-Dot Light-Emitting Devices by Effective Washing Process and Interfacial Energy Level Alignment. *ACS Appl. Mater. Interfaces* **2017**, *9* (21), 18054–18060. https://doi.org/10.1021/acsami.7b03382.

(23) Hoshi, K.; Chiba, T.; Sato, J.; Hayashi, Y.; Takahashi, Y.; Ebe, H.; Ohisa, S.; Kido, J. Purification of Perovskite Quantum Dots Using Low-Dielectric-Constant Washing Solvent "Diglyme" for Highly Efficient Light-Emitting Devices. *ACS Appl. Mater. Interfaces* **2018**, *10* (29), 24607–24612. https://doi.org/10.1021/acsami.8b05954.

(24) Pan, J.; Quan, L. N.; Zhao, Y.; Peng, W.; Murali, B.; Sarmah, S. P.; Yuan, M.; Sinatra, L.; Alyami, N. M.; Liu, J.; Yassitepe, E.; Yang, Z.; Voznyy, O.; Comin, R.; Hedhili, M. N.; Mohammed, O. F.; Lu, Z. H.; Kim, D. H.; Sargent, E. H.; Bakr, O. M. Highly Efficient Perovskite-Quantum-Dot Light-Emitting Diodes by Surface Engineering. *Advanced Materials* **2016**, *28* (39), 8718–8725. https://doi.org/10.1002/adma.201600784.

(25) Krieg, F.; Ochsenbein, S. T.; Yakunin, S.; ten Brinck, S.; Aellen, P.; Süess, A.; Clerc, B.; Guggisberg, D.; Nazarenko, O.; Shynkarenko, Y.; Kumar, S.; Shih, C.-J.; Infante, I.; Kovalenko, M. V. Colloidal CsPbX3 (X = Cl, Br, I) Nanocrystals 2.0: Zwitterionic Capping Ligands for Improved Durability and Stability. *ACS Energy Lett.* **2018**, *3* (3), 641–646. https://doi.org/10.1021/acsenergylett.8b00035.

(26) Vickers, E. T.; Graham, T. A.; Chowdhury, A. H.; Bahrami, B.; Dreskin, B. W.; Lindley, S.; Naghadeh, S. B.; Qiao, Q.; Zhang, J. Z. Improving Charge Carrier Delocalization in Perovskite Quantum Dots by Surface Passivation with Conductive Aromatic Ligands. *ACS Energy Lett.* **2018**, *3* (12), 2931–2939. https://doi.org/10.1021/acsenergylett.8b01754.

(27) Li, G.; Huang, J.; Li, Y.; Tang, J.; Jiang, Y. Highly Bright and Low Turn-on Voltage CsPbBr3 Quantum Dot LEDs via Conjugation Molecular Ligand Exchange. *Nano Res.* **2019**, *12* (1), 109–114. https://doi.org/10.1007/s12274-018-2187-5.

(28) Dai, J.; Xi, J.; Li, L.; Zhao, J.; Shi, Y.; Zhang, W.; Ran, C.; Jiao, B.; Hou, X.; Duan, X.; Wu, Z. Charge Transport between Coupling Colloidal Perovskite Quantum Dots Assisted by Functional Conjugated Ligands. *Angewandte Chemie International Edition* **2018**, *57* (20), 5754–5758. https://doi.org/10.1002/anie.201801780.

(29) Milliron, D. j.; Alivisatos, A. p.; Pitois, C.; Edder, C.; Fréchet, J. m. j. Electroactive Surfactant Designed to Mediate Electron Transfer Between CdSe Nanocrystals and Organic Semiconductors. *Advanced Materials*

2003, *15* (1), 58–61. https://doi.org/10.1002/adma.200390011.

(30) Liu, J.; Tanaka, T.; Sivula, K.; Alivisatos, A. P.; Fréchet, J. M. J. Employing End-Functional Polythiophene To Control the Morphology of Nanocrystal−Polymer Composites in Hybrid Solar Cells. *J. Am. Chem. Soc.* **2004**, *126* (21), 6550–6551. https://doi.org/10.1021/ja0489184.

(31) Skaff, H.; Sill, K.; Emrick, T. Quantum Dots Tailored with Poly(Para-Phenylene Vinylene). *J. Am. Chem. Soc.* **2004**, *126* (36), 11322–11325. https://doi.org/10.1021/ja047260r.

(32) Kim, H.; So, S.; Ribbe, A.; Liu, Y.; Hu, W.; Duzhko, V. V.; Hayward, R. C.; Emrick, T. Functional Polymers for Growth and Stabilization of CsPbBr3 Perovskite Nanoparticles. *Chem. Commun.* **2019**, *55* (12), 1833–1836. https://doi.org/10.1039/C8CC09343A.

(33) Liang, S.; He, S.; Zhang, M.; Yan, Y.; Jin, T.; Lian, T.; Lin, Z. Tailoring Charge Separation at Meticulously Engineered Conjugated Polymer/Perovskite Quantum Dot Interface for Photocatalyzing Atom Transfer Radical Polymerization. *J. Am. Chem. Soc.* **2022**, *144* (28), 12901–12914. https://doi.org/10.1021/jacs.2c04680.

(34) De Roo, J.; Ibáñez, M.; Geiregat, P.; Nedelcu, G.; Walravens, W.; Maes, J.; Martins, J. C.; Van Driessche, I.; Kovalenko, M. V.; Hens, Z. Highly Dynamic Ligand Binding and Light Absorption Coefficient of Cesium Lead Bromide Perovskite Nanocrystals. *ACS Nano* **2016**, *10* (2), 2071–2081. https://doi.org/10.1021/acsnano.5b06295.

(35) Liu, F.; Page, Z. A.; Duzhko, V. V.; Russell, T. P.; Emrick, T. Conjugated Polymeric Zwitterions as Efficient Interlayers in Organic Solar Cells. *Advanced Materials* **2013**, *25* (47), 6868–6873. https://doi.org/10.1002/adma.201302477.

(36) Liu, Y.; Page, Z. A.; Russell, T. P.; Emrick, T. Finely Tuned Polymer Interlayers Enhance Solar Cell Efficiency. *Angewandte Chemie International Edition* **2015**, *54* (39), 11485–11489. https://doi.org/10.1002/anie.201503933.

(37) Page, Z. A.; Liu, F.; Russell, T. P.; Emrick, T. Tuning the Energy Gap of Conjugated Polymer Zwitterions for Efficient Interlayers and Solar Cells. *Journal of Polymer Science Part A: Polymer Chemistry* **2015**, *53* (2), 327–336. https://doi.org/10.1002/pola.27349.

(38) Page, Z. A.; Liu, Y.; Puodziukynaite, E.; Russell, T. P.; Emrick, T. Hydrophilic Conjugated Polymers Prepared by Aqueous Horner–Wadsworth–Emmons Coupling. *Macromolecules* **2016**, *49* (7), 2526–2532. https://doi.org/10.1021/acs.macromol.5b02501.

(39) Duan, C.; Wang, L.; Zhang, K.; Guan, X.; Huang, F. Conjugated Zwitterionic Polyelectrolytes and Their Neutral Precursor as Electron Injection Layer for High-Performance Polymer Light-Emitting Diodes. *Advanced Materials* **2011**, *23* (14), 1665–1669. https://doi.org/10.1002/adma.201004661.

(40) Fang, J.; Wallikewitz, B. H.; Gao, F.; Tu, G.; Müller, C.; Pace, G.; Friend, R. H.; Huck, W. T. S. Conjugated Zwitterionic Polyelectrolyte as the Charge Injection Layer for High-Performance Polymer Light-Emitting Diodes. *J. Am. Chem. Soc.* **2011**, *133* (4), 683–685. https://doi.org/10.1021/ja108541z.

(41) Liu, Y.; Duzhko, V. V.; Page, Z. A.; Emrick, T.; Russell, T. P. Conjugated Polymer Zwitterions: Efficient Interlayer Materials in Organic Electronics. *Acc. Chem. Res.* **2016**, *49* (11), 2478–2488. https://doi.org/10.1021/acs.accounts.6b00402.

(42) Gillis, E. P.; Burke, M. D. A Simple and Modular Strategy for Small Molecule Synthesis: Iterative Suzuki−Miyaura Coupling of B-Protected Haloboronic Acid Building Blocks. *J. Am. Chem. Soc.* **2007**, *129* (21), 6716–6717. https://doi.org/10.1021/ja0716204.

(43) Li, J.; Grillo, A. S.; Burke, M. D. From Synthesis to Function via Iterative Assembly of N-Methyliminodiacetic Acid Boronate Building Blocks. *Acc. Chem. Res.* **2015**, *48* (8), 2297–2307. https://doi.org/10.1021/acs.accounts.5b00128.

(44) Lehmann, J. W.; Blair, D. J.; Burke, M. D. Towards the Generalized Iterative Synthesis of Small Molecules. *Nat Rev Chem* **2018**, *2* (2), 1–20. https://doi.org/10.1038/s41570-018-0115.

(45) Xu, C.; He, C.; Li, N.; Yang, S.; Du, Y.; Matyjaszewski, K.; Pan, X. Regio- and Sequence-Controlled Conjugated Topological Oligomers and Polymers via Boronate-Tag Assisted Solution-Phase Strategy. *Nat Commun* **2021**, *12* (1), 5853. https://doi.org/10.1038/s41467-021-26186-y.

(46) Li, J.; Ballmer, S. G.; Gillis, E. P.; Fujii, S.; Schmidt, M. J.; Palazzolo, A. M. E.; Lehmann, J. W.; Morehouse, G. F.; Burke, M. D. Synthesis of Many Different Types of Organic Small Molecules Using One Automated Process. *Science* **2015**, *347* (6227), 1221–1226. https://doi.org/10.1126/science.aaa5414.

(47) Lawrence, J.; Goto, E.; Ren, J. M.; McDearmon, B.; Kim, D. S.; Ochiai, Y.; Clark, P. G.; Laitar, D.; Higashihara, T.; Hawker, C. J. A Versatile and Efficient Strategy to Discrete Conjugated Oligomers. *J. Am. Chem. Soc.* **2017**, *139* (39), 13735–13739. https://doi.org/10.1021/jacs.7b05299.

(48) Knapp, D. M.; Gillis, E. P.; Burke, M. D. A General Solution for Unstable Boronic Acids: Slow-Release Cross-Coupling from Air-Stable MIDA Boronates. *J. Am. Chem. Soc.* **2009**, *131* (20), 6961–6963. https://doi.org/10.1021/ja901416p.

(49) Gonzalez, J. A.; Ogba, O. M.; Morehouse, G. F.; Rosson, N.; Houk, K. N.; Leach, A. G.; Cheong, P. H.-Y.; Burke, M. D.; Lloyd-Jones, G. C. MIDA Boronates Are Hydrolysed Fast and Slow by Two Different Mechanisms. *Nature Chem* **2016**, *8* (11), 1067–1075. https://doi.org/10.1038/nchem.2571.

(50) Li, B.; Li, J.; Fu, Y.; Bo, Z. Porphyrins with Four Monodisperse Oligofluorene Arms as Efficient Red Light-Emitting Materials. *J. Am. Chem. Soc.* **2004**, *126* (11), 3430–3431. https://doi.org/10.1021/ja039832y.

(51) Klaerner, G.; Miller, R. D. Polyfluorene Derivatives: Effective Conjugation Lengths from Well-Defined Oligomers. *Macromolecules* **1998**, *31* (6), 2007–2009. https://doi.org/10.1021/ma971073e.

(52) Bhattacharyya, S. A High Throughput Synthesis of N,N-Dimethyl Tertiary Amines. *Synthetic Communications* **2000**, *30* (11), 2001–2008. https://doi.org/10.1080/00397910008087249.

(53) Krieg, F.; Ong, Q. K.; Burian, M.; Rainò, G.; Naumenko, D.; Amenitsch, H.; Süess, A.; Grotevent, M. J.; Krumeich, F.; Bodnarchuk, M. I.; Shorubalko, I.; Stellacci, F.; Kovalenko, M. V. Stable Ultraconcentrated and Ultradilute Colloids of CsPbX3 (X = Cl, Br) Nanocrystals Using Natural Lecithin as a Capping Ligand. *J. Am. Chem. Soc.* **2019**, *141* (50), 19839–19849. https://doi.org/10.1021/jacs.9b09969.

(54) Krieg, F.; Sercel, P. C.; Burian, M.; Andrusiv, H.; Bodnarchuk, M. I.; Stöferle, T.; Mahrt, R. F.; Naumenko, D.; Amenitsch, H.; Rainò, G.; Kovalenko, M. V. Monodisperse Long-Chain Sulfobetaine-Capped CsPbBr3 Nanocrystals and Their Superfluorescent Assemblies. *ACS Cent. Sci.* **2021**, *7* (1), 135–144. https://doi.org/10.1021/acscentsci.0c01153.

(55) Imran, M.; Ijaz, P.; Baranov, D.; Goldoni, L.; Petralanda, U.; Akkerman, Q.; Abdelhady, A. L.; Prato, M.; Bianchini, P.; Infante, I.; Manna, L. Shape-Pure, Nearly Monodispersed CsPbBr3 Nanocubes Prepared

Using Secondary Aliphatic Amines. *Nano Lett.* **2018**, *18* (12), 7822–7831. https://doi.org/10.1021/acs.nanolett.8b03598.

(56) Almeida, G.; Goldoni, L.; Akkerman, Q.; Dang, Z.; Khan, A. H.; Marras, S.; Moreels, I.; Manna, L. Role of Acid–Base Equilibria in the Size, Shape, and Phase Control of Cesium Lead Bromide Nanocrystals. *ACS Nano* **2018**, *12* (2), 1704–1711. https://doi.org/10.1021/acsnano.7b08357.

(57) Imran, M.; Ijaz, P.; Goldoni, L.; Maggioni, D.; Petralanda, U.; Prato, M.; Almeida, G.; Infante, I.; Manna, L. Simultaneous Cationic and Anionic Ligand Exchange For Colloidally Stable CsPbBr3 Nanocrystals. *ACS Energy Lett.* **2019**, *4* (4), 819–824. https://doi.org/10.1021/acsenergylett.9b00140.

(58) Hens, Z.; Martins, J. C. A Solution NMR Toolbox for Characterizing the Surface Chemistry of Colloidal Nanocrystals. *Chem. Mater.* **2013**, *25* (8), 1211–1221. https://doi.org/10.1021/cm303361s.

(59) Fytas, G.; Nothofer, H. G.; Scherf, U.; Vlassopoulos, D.; Meier, G. Structure and Dynamics of Nondilute Polyfluorene Solutions. *Macromolecules* **2002**, *35* (2), 481–488. https://doi.org/10.1021/ma011416f.

(60) Nagaoka, Y.; Hills-Kimball, K.; Tan, R.; Li, R.; Wang, Z.; Chen, O. Nanocube Superlattices of Cesium Lead Bromide Perovskites and Pressure-Induced Phase Transformations at Atomic and Mesoscale Levels. *Advanced Materials* **2017**, *29* (18), 1606666. https://doi.org/10.1002/adma.201606666.

(61) Rainò, G.; Becker, M. A.; Bodnarchuk, M. I.; Mahrt, R. F.; Kovalenko, M. V.; Stöferle, T. Superfluorescence from Lead Halide Perovskite Quantum Dot Superlattices. *Nature* **2018**, *563* (7733), 671–675. https://doi.org/10.1038/s41586-018-0683-0.

(62) Baranov, D.; Fieramosca, A.; Yang, R. X.; Polimeno, L.; Lerario, G.; Toso, S.; Giansante, C.; Giorgi, M. D.; Tan, L. Z.; Sanvitto, D.; Manna, L. Aging of Self-Assembled Lead Halide Perovskite Nanocrystal Superlattices: Effects on Photoluminescence and Energy Transfer. *ACS Nano* **2021**, *15* (1), 650–664. https://doi.org/10.1021/acsnano.0c06595.

Graphic for TOC